

## Impedance Boundary Condition for Lattice Boltzmann Model

Chenghai Sun\*, Franck Pérot, Raoyang Zhang, David M. Freed and Hudong Chen

*Exa Corporation, 55 Network drive, Burlington, MA 01803, USA.*

Received 31 October 2011; Accepted (in revised version) 26 January 2012

Available online 29 August 2012

---

**Abstract.** A surface based lattice Boltzmann impedance boundary condition (BC) using Ozyoruk's model [J. Comput. Phys., 146 (1998), pp. 29-57] is proposed and implemented in PowerFLOW. In Ozyoruk's model, pressure fluctuation is directly linked to normal velocity on an impedance surface. In the present study, the relation between pressure and normal velocity is realized precisely by imposing a mass flux on the surface. This impedance BC is generalized and can handle complex geometry. Combined with the turbulence model in the lattice Boltzmann solver PowerFLOW, this BC can be used to model the effect of a liner in presence of a complex 3D turbulent flow. Preliminary simulations of the NASA Langley grazing flow tube and Kundt tube show satisfying agreement with experimental results.

**AMS subject classifications:** 76Q05

**Key words:** Acoustics, impedance, lattice Boltzmann.

---

### 1 Introduction

Sound absorbing materials are widely used in various industries to reduce noise emission. For example in modern turbofan engines, the inlet wall is treated with acoustic liners. Highway and railway noise barriers often use acoustic treatments for reducing community noise issues. These sound absorbing materials are composed of porous media allowing non-zero normal velocity at the surface. Considering the difficulty to model the flow and the acoustic propagation inside porous media, an acoustic liners are usually handled with macroscopic boundary conditions imposed in the frequency domain, consisting of a quantity called impedance, defined as

$$\hat{p}(\mathbf{x}, \omega) = Z(\omega) \hat{\mathbf{u}}(\mathbf{x}, \omega) \cdot \mathbf{n}(\mathbf{x}), \quad (1.1)$$

---

\*Corresponding author. *Email addresses:* chenghai@exa.com (C. Sun), perot@exa.com (F. Pérot), raoyang@exa.com (R. Zhang), dmfreed@exa.com (D. Freed), hudong@exa.com (H. Chen)

where  $\hat{p}$  is the acoustic pressure,  $\hat{\mathbf{u}}$  is the acoustic velocity and  $\mathbf{n}$  is the mean surface normal. The impedance is a frequency-dependent complex quantity given by

$$Z(\omega) = R(\omega) + iX(\omega), \quad (1.2)$$

where  $R(\omega)$  and  $X(\omega)$  are the resistance and reactance, respectively, of the liner. These are properties of the material and can be measured experimentally in a Kundt tube. The impedance  $Z$  given by Eq. (1.1) provides a relation between acoustic pressure and velocity at the surface in the frequency domain. In order to be used as a boundary condition in the physical domain of a time-explicit computational fluid dynamics (CFD) simulation, this relation has to be transformed into time domain. Mathematically, the time-domain equivalent of the frequency domain impedance condition can be derived by taking the inverse Fourier transform. However, due to the convolution integral, long time history of the acoustic velocity would be required. Ozyoruk et al. [1] proposed an efficient implementation of the above impedance boundary condition in the time domain by using the  $z$ -transform. Taking advantage of the time-shifting and convolution properties of the  $z$ -transform, the implementation only needs to store values of pressure and velocity at a few previous time steps. The simulations of the NASA Langley grazing flow tube case using this model [1–3] showed good agreement with experimental data. Toutant et al. [4] applied this scheme within a lattice Boltzmann method (LBM) flow solver and also showed similarly good correlations to the experiment. However, this implementation of the impedance boundary condition is limited to a wall boundary perfectly aligned with the cell boundaries of the underlying LBM grid. Hence Toutant's approach is not suitable for treating complex geometries with inclined or curved boundaries.

In the present paper, we extend the previous work to provide a surface based impedance BC for arbitrary wall boundary geometry which incorporates Ozyoruk's model in a generalized LBM flow solver PowerFLOW. The effective LB boundary treatment in PowerFLOW provides the ability to impose desired boundary conditions, for example frictionless BC, on complex geometries [5]. The advanced Very-Large-Eddy-Simulation (VLES) turbulence model applied in PowerFLOW [6,7] further enables accurate simulations of high Reynolds number turbulent flows. Therefore realization of the generalized time-domain impedance BC in PowerFLOW makes possible for the first time quantitative analyzes of more realistic aero-acoustic problems besides acoustic liners represented by Ozyoruk's model.

## 2 Impedance boundary condition

For the constant depth ceramic tubular liner (CT73) [8] the following impedance function is proposed in [1] by curve fitting the experimental data:

$$\frac{Z(\omega)}{\rho_0 c_0} = r_1 + \frac{r_2 - r_1}{1 + i\omega r_3} + \frac{i\omega r_4}{(1 - \omega^2/r_6^2) + i\omega r_5} + i\omega r_7, \quad (2.1)$$

where  $c_0$  is the speed of sound and the values for the  $r_i$  constants are given in [1]. This model satisfies all the fundamental conditions for a physically admissible impedance model listed by Rienstra [9]: causality, reality, and passivity for  $Z(\omega)$ .

Translation into the time domain is obtained via z-transform. Let  $f(t)$  be a continuous function and  $F(z) = \mathcal{Z}(f(t))$  be corresponding z-transform. Let  $f(n\Delta t)$  represent the  $n^{th}$  time-discrete sample of  $f(t)$ , then the time shifting property is given by

$$\mathcal{Z}\{f((n-1)\Delta t)\} = z^{-1} \mathcal{Z}\{f(n\Delta t)\} = z^{-1}F(z). \tag{2.2}$$

The convolution property is:

$$\mathcal{Z}\{f(n\Delta t) * g(n\Delta t)\} = F(z)G(z). \tag{2.3}$$

Using the time-shifting property and a first order backward difference, the time derivative operator can be written as

$$i\omega \equiv \frac{\partial}{\partial t} \equiv \frac{1-z^{-1}}{\Delta t}. \tag{2.4}$$

Evaluating  $i\omega$  in (2.1) using (2.3), one obtains the impedance model in z-domain

$$\frac{Z(z)}{\rho_0 c_0} = \frac{\sum_{l=0}^4 a_l z^{-l}}{-\sum_{k=0}^3 b_k z^{-k}}, \tag{2.5}$$

where  $b_0 = -1$ ,  $a$ 's and  $b$ 's are constants determined by  $r$ 's in (2.1).

Myers [10] extended Eq. (1.1) to the impedance boundary condition in presence of flow, assuming that the deformation of the soft wall is small in response to an incident acoustic wave from the fluid, and that this acoustic field is a small perturbation to the mean base flow:

$$i\omega \hat{p}(\mathbf{x}, \omega) + \mathbf{u}_0(\mathbf{x}) \cdot \nabla \hat{p}(\mathbf{x}, \omega) - \mathbf{n} \cdot (\mathbf{n} \cdot \nabla \mathbf{u}_0(\mathbf{x})) \hat{p}(\mathbf{x}, \omega) = i\omega Z(\omega) \hat{\mathbf{u}}(\mathbf{x}, \omega) \cdot \mathbf{n}(\mathbf{x}). \tag{2.6}$$

This equation can be written in the z domain using the z-transform properties:

$$\frac{1-z^{-1}}{\Delta t} P(\mathbf{x}, z) + \mathbf{u}_0(\mathbf{x}) \cdot \nabla P(\mathbf{x}, z) - \mathbf{n} \cdot (\mathbf{n} \cdot \nabla \mathbf{u}_0(\mathbf{x})) P(\mathbf{x}, z) = \frac{1-z^{-1}}{\Delta t} Z(z) \mathbf{U}(\mathbf{x}, z) \cdot \mathbf{n}(\mathbf{x}). \tag{2.7}$$

For flat-wall boundary with a uniform mean flow it simplifies to:

$$\frac{1-z^{-1}}{\Delta t} P(\mathbf{x}, z) + \mathbf{u}_0 \cdot \nabla P(\mathbf{x}, z) = \frac{1-z^{-1}}{\Delta t} Z(z) \mathbf{U}(\mathbf{x}, z) \cdot \mathbf{n}(\mathbf{x}). \tag{2.8}$$

Substituting (2.5) in (2.8) for  $Z(z)$  and taking the inverse z-transform, the time-domain impedance condition can be written:

$$\frac{p^{n+1} - p^n}{\Delta t} + u_0 \frac{\partial p^{n+1}}{\partial x} - \sum_{k=1}^3 b_k \left[ \frac{p^{n+1-k} - p^{n-k}}{\Delta t} + u_0 \frac{\partial p^{n+1-k}}{\partial x} \right] = \sum_{l=0}^4 a_l \left[ \frac{v_n^{n+1-l} - v_n^{n-l}}{\Delta t} \right], \tag{2.9}$$

where  $v_n = \mathbf{u} \cdot \mathbf{n}$ . The normal velocity can be written explicitly by rearranging this equation:

$$v_n^{n+1} = \frac{p^{n+1}}{a_0} - \sum_{k=0}^3 p^{n-k} \left[ \frac{b_{k+1} - b_k}{a_0} \right] - \sum_{l=0}^4 v_n^{n-l} \left[ \frac{a_{l+1} - a_l}{a_0} \right] - \frac{u_0 \Delta t}{a_0} \sum_{k=0}^3 b_k \left[ \frac{\partial p^{n+1-k}}{\partial x} \right], \quad (2.10)$$

with  $a_5 = 0$  and  $b_4 = 0$ .

Eq. (2.10) is used herein to provide the impedance BC as follows: (1) the pressure at the wall is determined in the usual way; (2) the normal velocity is computed from (2.10) as a function of the current pressure and the previous four-time-step history of both the pressure and the normal velocity at the wall; (3) the new normal velocity is then enforced as the wall boundary condition at the next time step.

### 3 LBM model

The 3D 19-speed LBM (D3Q19) [14] used in current study is:

$$f_i(\mathbf{x} + \mathbf{c}_i, t + \Delta t) = f_i(\mathbf{x}, t) - \frac{1}{\tau} (f_i(\mathbf{x}, t) - f_i^{eq}(\mathbf{x}, t)). \quad (3.1)$$

Here  $f_i(\mathbf{x}, t)$  is the particle density distribution function and  $\tau$  is the single relaxation time. The equilibrium distribution function  $f_i^{eq}(\mathbf{x}, t)$  has the following 3rd order form:

$$f_i^{eq}(\mathbf{x}, t) = \rho w_i \left[ 1 + \frac{\mathbf{c}_i \cdot \mathbf{u}}{T_0} + \frac{(\mathbf{c}_i \cdot \mathbf{u})^2}{2T_0^2} - \frac{\mathbf{u}^2}{2T_0} + \frac{(\mathbf{c}_i \cdot \mathbf{u})^3}{6T_0^3} - \frac{(\mathbf{c}_i \cdot \mathbf{u})\mathbf{u}^2}{2T_0^2} \right], \quad (3.2)$$

with  $w_0 = 1/3$  for stop state,  $w_i = 1/18$  for states in Cartesian directions and  $w_i = 1/36$  for states in bi-diagonal directions. Here  $T_0 = 1/3$  is the constant lattice temperature. The hydrodynamic quantities  $\rho$  and  $\rho \mathbf{u}$  are the zeroth and first order moments of the distribution functions respectively:

$$\rho(\mathbf{x}, t) = \sum_i f_i(\mathbf{x}, t), \quad \rho(\mathbf{x}, t) \mathbf{u}(\mathbf{x}, t) = \sum_i \mathbf{c}_i f_i(\mathbf{x}, t). \quad (3.3)$$

By Chapman-Enskog expansion, the evolution of Eq. (3.1) matches the Navier-Stokes equations, with pressure and sound speed  $c_0$  given by:

$$p(\mathbf{x}, t) = c_0^2 \rho(\mathbf{x}, t), \quad c_0 = \frac{1}{\sqrt{3}} \frac{\Delta x}{\Delta t}. \quad (3.4)$$

In general, standard wall boundary conditions impose zero normal velocity for both no-slip and slip impermeable walls. Please see [5] for details of the generalized volumetric BCs used in PowerFLOW. As described above, the impedance BC requires a normal velocity determined by Eq. (2.10) to be imposed at the surface. This is achieved by adding a corresponding mass flux on the surface. The mass flux across a surface element (surfel)

$\alpha$  is  $\rho v_n^\alpha S_\alpha$ , where  $S_\alpha$  is the area of the surfel. Such a surface mass flux is isotropically distributed to the out-going particles from the surfel. That is to say, after realizing regular impermeable surfel BCs, an additional impedance dependent  $\delta f$  is added to the out-going particle distributions in each surfel  $\alpha$ :

$$\delta f_i^\alpha(\mathbf{x}, t) = \frac{\rho_\alpha v_n^\alpha S_\alpha}{\sum_{j, \mathbf{c}_j \cdot \mathbf{n} > 0} V_j^\alpha} \quad \text{if } \mathbf{c}_i \cdot \mathbf{n} > 0; \quad \delta f_i^\alpha(\mathbf{x}, t) = 0 \quad \text{otherwise,} \quad (3.5)$$

where  $\mathbf{n}$  is the normal of the surfel  $\alpha$ ,  $v_n^\alpha$  is the solution of normal velocity from Eq. (2.10),  $\rho_\alpha$  is the density sampled from the surrounding cells which interact with the surfel, and  $V_j^\alpha$  is the "pgram volume" defined as the volume of the domain of the parallelepiped extruded from the surfel in the direction of  $\mathbf{c}_j$ , i.e.  $V_j^\alpha = |\mathbf{c}_j \cdot \mathbf{n}| S_\alpha \Delta t$  (see details in [5]). The volume of the overlapping domain of the parallelepiped and the cell  $\mathbf{x}$  is defined as  $V_j^\alpha(\mathbf{x})$ , and obviously,

$$\sum_{\mathbf{x}} V_j^\alpha(\mathbf{x}) = V_j^\alpha. \quad (3.6)$$

It is straightforward to show that the total mass flux from the surfel  $\alpha$  to fluid cells is

$$\sum_{i, \mathbf{x}} \delta f_i^\alpha(\mathbf{x}, t) V_i^\alpha(\mathbf{x}) = \rho_\alpha v_n^\alpha S_\alpha. \quad (3.7)$$

Therefore the desired mass flux is precisely achieved.

It is worth pointing out that such an impedance boundary treatment does not alter surface tangential momentum flux. Its realization is independent of the existing fluid flow boundary conditions. As long as the impedance induced surface mass flux could be accurately controlled, this impedance BC is generally applicable to any LBM boundary models. To our best knowledge, however, the surfel based volumetric BC [5] used in PowerFLOW is the only approach achieving exact frictionless BC on arbitrary geometries, which is essential to simulations of practical turbulent fluid flows. Based on this generalized volumetric BC, our impedance BC is naturally generalized and applicable to simulations of engineering problems.

## 4 Numerical results

Two validation studies are described in this section. First, the LBM surfel-based impedance boundary is characterized in a virtual impedance tube to verify that under pure acoustics (no flow) conditions, the present implementation recovers the normal incidence impedance properties of the ceramic liner CT73. The second study uses the well-known NASA Langley grazing incidence impedance tube case [8], which includes a mean flow together with tangentially incident acoustics, and is a widely used validation case in the open literature [1, 2, 4].

#### 4.1 Normal impedance tube

The complex surface impedance  $Z_s$  of a material can be directly measured in a normal-incidence impedance tube (also called a Kundt tube) [11–13] using a two-microphone method. A schematic representation of a cylindrical impedance tube is given in Fig. 1. On the left side of the tube, a broadband white noise source generates pressure waves traveling toward the material to be acoustically characterized. At the interface between the air and the material, the incident waves are either transmitted or reflected. The reflected waves combine with the incident ones forming standing waves with amplitude and phase variation along the length of the tube that is a function of the material impedance. Due to continuity of the variables at the interface  $x=0$ , the complex surface impedance is found by measuring the pressure  $p_1(t) = p(x_1, t)$  and  $p_2(t) = p(x_2, t)$  at two points  $x_1$  and  $x_2$  inside the tube and using the following expression:

$$\frac{Z_s}{Z_0} = i \frac{\hat{h}_{12} \sin(Kl) - \sin[K(l-s)]}{\cos[K(l-s)] - \hat{h}_{12} \cos(Kl)}, \quad (4.1)$$

with  $s = x_1 - x_2$  and  $x_2 = l$ ,  $Z_0 = \rho_0 c_0$  the air characteristic impedance,  $c_0$  the speed of sound,  $\rho_0$  the air density,  $K = \omega / c_0$  the wave number. The complex transfer function  $h_{12}$  between  $p_1$  and  $p_2$  is given by the following expression for which the hatted variables correspond to the frequency domain Fourier transform operation:

$$\hat{h}_{12} = \frac{1}{K} \sum_k \frac{\hat{p}_{2,k}}{\hat{p}_{1,k}}. \quad (4.2)$$

The subscript  $k$  corresponds to the Fourier transform operation applied to  $k^{th}$  subset time interval of the complete signals (called time windows). In a discrete form, this leads to  $p_{j,k} = p(x_j, I_k)$  with  $I_k = [N(k-1) + 1, Nk]$ , where  $N$  is the number of samples in the time window and  $j=1$  or  $j=2$ . The complex surface impedance  $Z_s(\omega)$  is commonly expressed as a function of its real and imaginary parts, the resistance  $R(\omega)$  and the reactance  $X(\omega)$ , respectively. This work considers a passive material characterized by  $R(\omega) > 0$  (i.e. positive resistance) [9]. The material absorption coefficient  $\alpha(\omega)$  is defined by:

$$\alpha(\omega) = 1 - \left| \frac{1 - Z_s}{1 + Z_s} \right|^2. \quad (4.3)$$

To assess the effect of the surfel-based boundary condition impedance model on acoustics propagation, a 3-D circular impedance tube (Fig. 1) is simulated using VLES. Similarly to an experiment, a white noise signal is applied on the left face of the tube and the boundary condition to be characterized imposed on the right one. Two simulations using two boundary conditions are applied to the right face. First, a rigid wall is used in order to verify the numerical dissipation of the system and to check that a near-zero absorption coefficient is recovered (Setup A). Second, the CT73 surfel-based condition is

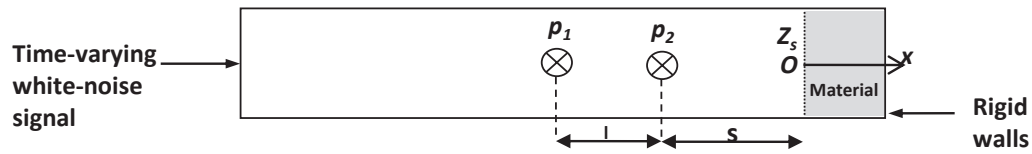


Figure 1: Schematic representation of a cylindrical impedance tube.

used and compared to the expression (2.1) derived from a curve fitting of the measured complex surface impedance [1] (Setup B).

The cylindrical wall of the tube is defined as a frictionless BC. The length of the tube is  $L=0.772$  m and the diameter  $D=0.0515$  m. The frequency range for a valid usage of this tube is then 100Hz to 3000Hz. A uniform grid resolution corresponding to one hundred points per wavelength at  $f=3000$  Hz, i.e.  $\Delta x=1.1$  mm, is used. The time step is  $\Delta t=3.33 \times 10^{-6}$  s and the simulations run for a physical time of  $T=2$  s which is sufficient for the results to evolve beyond the start-up transient period and provide meaningful statistics. The complex Fourier transform is performed using a Fast Fourier transform algorithm (FFTW) applied to time windows composed of  $N=2^9$  samples and using  $N=2^{17}$  samples of the simulated signal. Pressure time histories are recorded inside the tube at two virtual microphones  $p_1(x_1, t)$  and  $p_2(x_2, t)$ .

As seen in Fig. 2, the absorption coefficient corresponding to Setup A (black dots) is close to zero over the frequency range. This result shows that the dissipation of the numerical setup is almost negligible and validates the implementation of the two-microphone method. The comparison for Setup B between the experimental results in red and the simulation results in blue presents a satisfying agreement. The shape and the levels of the absorption coefficient are similar. The slight overestimation of the absorption in the simulation can be attributed to the residual dissipation of the system. Some peaks in the simulation are observed at 400Hz and 2200Hz and are related to specific tube modes captured in the impedance tube. Such a behavior is also observed when performing real measurements and usually the absorption is represented with a wider bandwidth in order to avoid this effect.

The real and imaginary parts of the complex surface impedance are represented in Fig. 3 for Setup B. As expected, the real part is positive since the material is passive both experimentally and numerically. The overall comparison between experiments and prediction also highlight satisfying results showing that the correct effect of the boundary conditions on the standing modes is recovered in the simulation.

## 4.2 NASA Langley flow-impedance tube

The NASA Langley flow-impedance tube [8] has been simulated using a  $661 \times 41$  2D grid, providing a number of points per wave-length  $NPPW=60$  at 3000 Hz. The physical size of the tube is  $33 \times 2$  inches. The lower wall has a ceramic liner patch starting at 8.25"

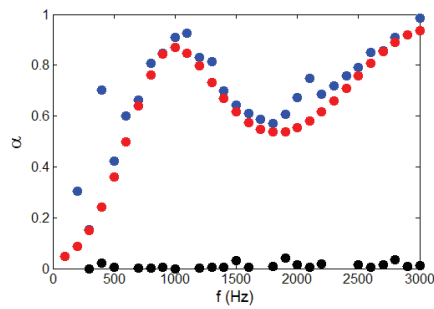


Figure 2: Absorption coefficient as a function of the frequency. Red: CT73 experiments; Blue: CT73 LBM simulation; Black: Rigid wall simulation.

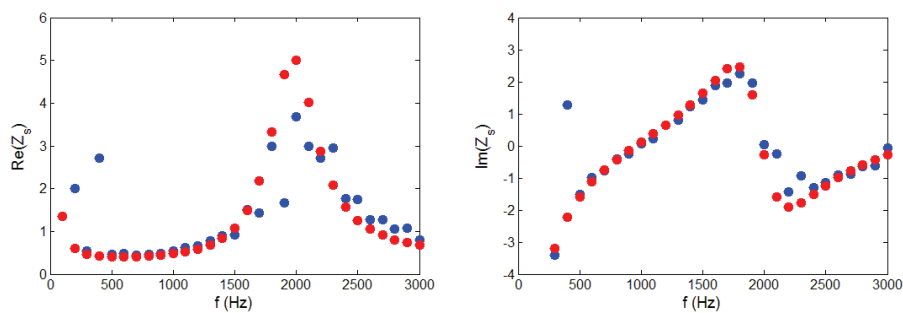


Figure 3: Real and Imaginary parts of the CT73 complex surface impedance. Red: experiments; Blue: LBM simulation.

from the inlet and extending to 23.5" from the inlet (indicated by the pink area at the lower wall in Fig. 4). Frictionless boundary conditions are imposed at the solid walls for direct numerical simulations (DNS) and the impedance boundary condition is used for

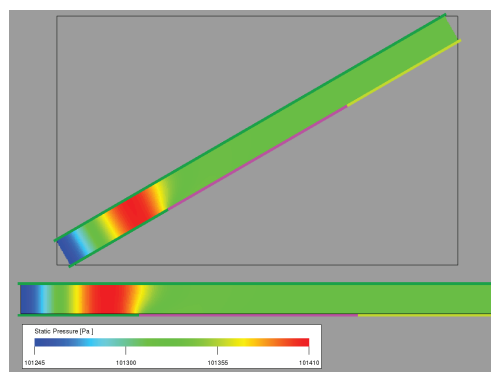


Figure 4: Pressure snap shot for DNS simulations at  $Ma = 0$ . Comparison of lattice-aligned and 30deg inclined channels.

the ceramic liner. An acoustic plane wave is generated at the inlet:

$$p_{in} = p_0 + \epsilon \sin(\omega t), \quad u_{in} = u_0 + \frac{\epsilon}{\rho_0 c_0} \sin(\omega t), \quad v_{in} = 0, \quad (4.4)$$

where  $p_0$  and  $\rho_0$  are ambient pressure and density,  $c_0$  is the speed of sound, and  $u_0 = Ma * c_0$ .

The sound pressure level (SPL) is calculated by:

$$SPL = 20 \log \left( \frac{p_{rms}}{p_{ref}} \right), \quad p_{rms}^2 = \frac{1}{t_2 - t_1} \int_{t_1}^{t_2} (p - p_0)^2 dt, \quad p_{ref} = 2 \times 10^{-5} \text{ Pa}. \quad (4.5)$$

A sound level of  $SPL = 130$  dB was set, for which  $\epsilon = 89.44$  Pa. Three types of cases are tested: (1) DNS of lattice aligned channel, (2) DNS with the channel inclined by 30 deg, and (3) simulations of lattice aligned channel with the VLES turbulence model [6,7]. For the DNS cases, relaxation time  $\tau$  is set to 0.504. For each type of case, simulations are carried out at mean flow Mach numbers of 0.0, 0.1, and 0.3 (only at Mach number 0.3 for turbulence modeling) and for frequencies ranging from 0.5 to 3.0 kHz with 0.5 kHz increment. SPL is measured along the upper wall and compared with experimental data [8].

Fig. 4 shows snapshots of pressure for the DNS lattice-aligned and inclined channels at  $Ma = 0$ . Good agreement indicates the grid orientation independence of the approach.

Fig. 5 shows the comparison of the upper wall SPL results of lattice-aligned and inclined DNS simulations with experimental data for zero mean flow ( $Ma = 0$ ). The symbols indicate the experimental SPL on the upper wall. The difference between the lattice aligned and inclined channel simulations is small, and both agree well with measurement data.

Same comparison as Fig. 5 but with mean flow ( $Ma = 0.1$ ) is shown in Fig. 6. Again, both the lattice-aligned and inclined simulations have good agreement with experimental data.

For  $Ma = 0.3$ , lattice-aligned DNS and turbulence simulations are compared with experimental data in Fig. 7. In turbulence simulations, the so-called slip wall boundary condition described in [5], together with turbulent wall function, are applied on solid walls to solve under-resolved turbulent boundary layer. The Reynolds number is  $Re = 2 \times 10^5$ . The difference between DNS and turbulence results is insignificant and both agree well with experiment.

## 5 Discussions

A generalized surfel-based algorithm is proposed to realize the impedance boundary condition for arbitrary geometry. The algorithm relies on the precise control of mass flux

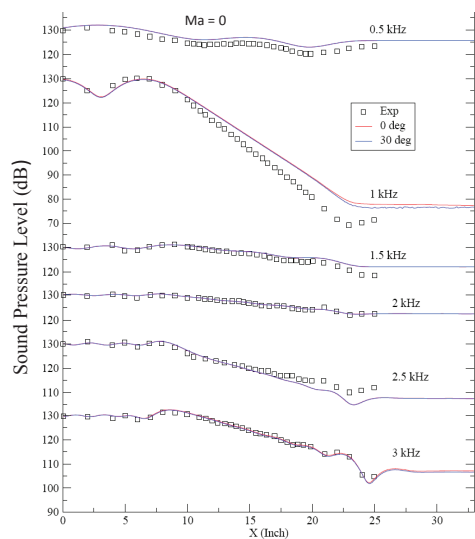


Figure 5:  $Ma=0$ . Comparison of lattice-aligned and inclined DNS simulations with experiment data.

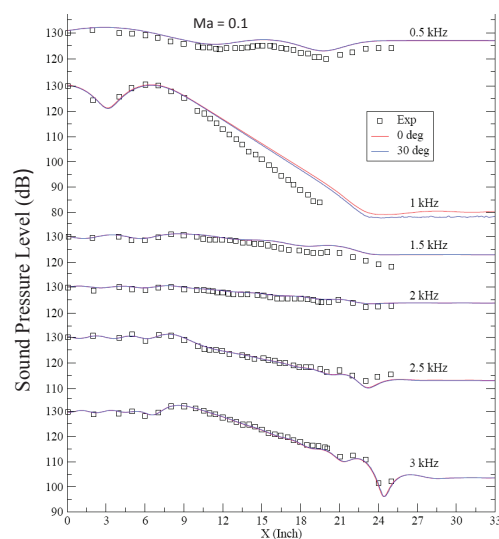


Figure 6:  $Ma=0.1$ . Comparison of lattice-aligned and inclined DNS simulations with experiment data.

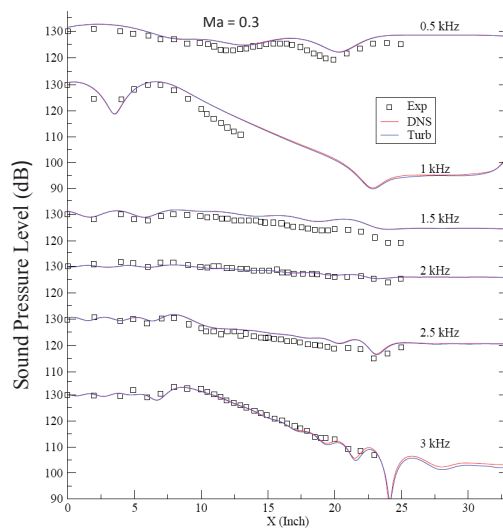


Figure 7:  $Ma=0.3$ . Comparison of DNS and turbulence simulations of lattice-aligned channel with experiment data.

through the impedance wall. After computing the local normal surface fluid velocity determined by the impedance equation (2.10), the impedance BC is achieved by introducing the necessary additional mass flux according to the normal velocity on impedance surface. It is demonstrated that the approach is capable of treating complex geometries and providing lattice orientation independent solutions.

The numerical measurement of real part and imaginary part of the complex impedance, as well as the absorption coefficient, in normal impedance tube are in very good agreement with experimental data, which verifies the accuracy of Ozyoruk's impedance model as well as our numerical scheme and corresponding implementation. Simulations of The NASA Langley flow-impedance tube correlate well with experiment, as shown for Mach numbers up to 0.3. Due to the Mach limitation of the standard 19s LB model used in our study, our simulations with  $Ma=0.5$  encounter numerical instability. This issue certainly could be addressed by using higher order LB models such as 39-speed LBM [15,16].

Since our impedance BC is generalized with no dependence on fluid model nor impedance material, it should work in simulations with more general flow situations, such as turbulent flow. Our turbulent simulation results of the NASA Langley flow-impedance tube demonstrated its applicability. More rigorous validations will be performed when realistic turbulence impedance experimental data is available.

In principal, our impedance model works for any impedance material as long as it can be properly formulated as fractional polynomials (2.5) in  $z$  domain as proposed in [1]. However, fitting the measurement data into this fractional polynomials might be challenging because causality, reality, and passivity listed by Rienstra [9] can not be always satisfied. Violation of these constrains could result in unphysical behavior or numerical instability. For an impedance material which cannot be expressed in this way, a different scheme is then required.

## Acknowledgments

The authors would like to thank Dr. A. Toutant for helpful discussions.

## References

- [1] Y. Ozyouk, L. N. Long, and M. G. Jones, Time-domain numerical simulation of a flow impedance tube, *J. Comput. Phys.*, 146 (1998), 29-57.
- [2] G. Delattre, E. Manoha, S. Redonnet, and P. Sagaut, Time-domain simulation of sound absorption on curved wall, 13th AIAA/CEAS Aeroacoustics conference, Rome, Italy, AIAA-2007-3493 (2007).
- [3] X. Y. Li and X. D. Li, Construction and validation of a broadband time domain impedance boundary condition, 17th AIAA/CEAS Aeroacoustics conference, Portland, Oregon, AIAA-2011-2870 (2011).
- [4] A. Toutant and P. Sagaut, Lattice Boltzmann simulations of impedance tube flows, *Computers & Fluids*, 38(2) (2009), 458-465.
- [5] H. Chen, C. Teixeira, and K. Molving, Realization of fluid boundary conditions via discrete Boltzmann dynamics, *Int. J. of Mod. Phys. C.*, 9(8) (1998), 1281-1292.
- [6] H. Chen, S. Kandasamy, S. Orszag, R. Shock, S. Succi, and V. Yakhot, Extended Boltzmann kinetic equation for turbulent flows, *Science*, 301 (2003), 633-636.

- [7] H. Chen, S. A. Orszag, I. Staroselsky, and S. Succi, Expanded analogy between Boltzmann theory of fluids and turbulence, *J. Fluid. Mech.*, 519 (2004), 301-314.
- [8] T. L. Parrott, W. R. Watson, and M. G. Jones, Experimental validation of a two-dimensional shear-flow model for determining acoustic impedance, *NASA Technical Paper*, 2679 (1987), 1-46.
- [9] S. W. Rienstra, 1-D Reflection at an impedance wall, *J. of Sound and Vibration*, 125(1) (1988), 43-51.
- [10] M. K. Myers, On the acoustic boundary condition in the presence of flow, *J. of Sound and Vibration*, 71(3) (1980), 429-434.
- [11] J. F. Allard, *Propagation of Sound in Porous Media: Modeling Sound Absorbing Materials*, Elsevier Editions, 1993.
- [12] C. K. W. Tam and L. Auriault, Time-domain impedance conditions for computational aeroacoustics, *AIAA Journal*, 34(5) (1996), 917.
- [13] G. A. Brès, F. Pérot, and D. Freed, Properties of the lattice-Boltzmann method for acoustics, 13th AIAA/CEAS aeroacoustics conference, Miami, Florida, AIAA 2009-3395 (2009).
- [14] Y. H. Qian, D. d'Humières, and P. Lallemand, Lattice BGK models for Navier-Stokes equation, *Europhys. Lett.*, 17 (1992), 479-484.
- [15] X. Nie, X. Shan, and H. Chen, Lattice-Boltzmann/Finite-Difference hybrid simulation of transonic flow, 47th AIAA Aerospace Science Meeting Including The Horizons Forum and Aerospace Exposition, Orlando, Florida, AIAA 2009-139 (2009).
- [16] X. Shan, X.-F. Yuan, and H. Chen, Kinetic theory representation of hydrodynamics: A way beyond the Navier-Stokes equation, *J. Fluid Mech.*, 550 (2006), 413-441.